Freie Universität Berlin

Advanced Laboratory Course

Pulsed Nuclear Magnetic Resonance (NMR)

Rocky Kamen-Rubio and Federico Porcelli (Group M9)

Supervisor: Elisabetta Di Gregorio

Experiment conducted on 21.11.2024

Abstract

(insert abstract)

Contents

1 Introduction

1.1 What is NMR?

NMR (Nuclear Magnetic Resonance) is phenomenon in which atomic nuclei interact with electromagnetic radiation due to their magnetic dipole. It has applications in material measurement, especially in medicine with Magnetic Resonance Imaging (MRI machines).

From quantum mechanical theory, recall that protons and neutrons have a property called "spin", which behaves like angular momentum. Thus the nuclei have spin, namely a spin system composed of protons and neutrons, and the interaction strength of the EM radiation depends on spin (i.e. quantum state) and type of nucleus (element). As a consequence, nuclei with L = 0 (where L is the angular momentum quantum number of the nucleus) do not interact, and are thus "invisible", e.g. ^{12}C, ^{16}O.

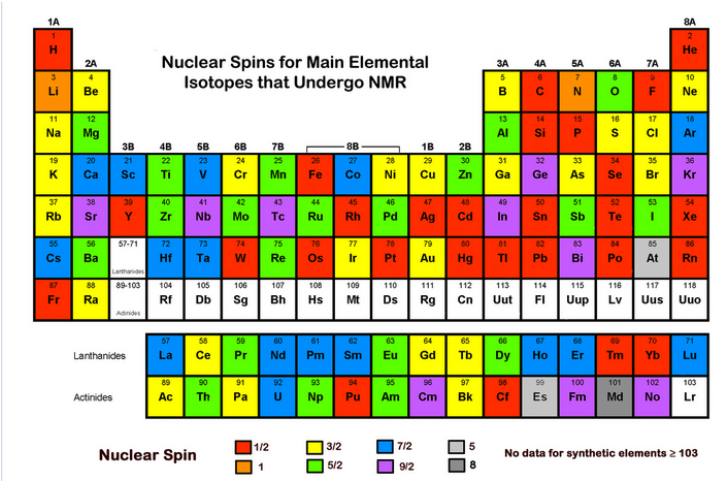

Figure 1: Table illustrating nuclear spins for different elements [**mri_questions_nuclear_spin**]

The gyromagnetic ratio (γ) is defined as the ratio of the magnetic moment to the angular momentum.

$$\gamma = \frac{\mu}{L}$$

More intuitively, this can be thought of as "how strongly a given configuration interacts with a B-field", or "how much magnetic moment you get per angular momentum". The gyromagnetic ratio of a proton $\gamma_{proton} \approx 2.68 s^{-1} T^{-1}$ (there is some theory around why this is the value but it is not relevant right now). Recall as well that the energy of a magnetic moment μ in a magnetic field B is $-\mu B$

1.2 What happens to a nuclear spin in a magnetic field (Zeeman splitting, Larmor precession, Larmor frequency)

A magnetic field will cause the particles to align their magnetic dipoles with the field. They can align with the field, in what is called the α state, or antiparellel to it, in what we call the β state. The difference between these two energy states will be

$$\Delta E = \frac{\gamma \hbar B_0}{2\pi}$$

Note that this split is proportional to the applied magnetic field. When we consider that spin quantum number $m_I \in -I, ..., I$, we get

$$E = E_0 - \frac{\hbar \gamma B_0 m_I}{2\pi}$$

Larmor procession is procession that will occur by the magnetic moments around the applied B-field. This behaves as expected with a classical gyroscope, we call its frequency the **Larmor frequency** and it is

$$\omega_L = \gamma B_0$$

1.3 Ensemble of spins.

Without an external magnetic field, the sum of all magnetic moments cancels, and thus no population difference between two spin states can exist (equal distribution of spin up-spin down particles). However, when we introduce an external magnetic field, a difference in the population of two spin states occurs, which results in a net magnetization parallel to the applied field.

The energy difference of states leads to a difference in population

$$\frac{N_{upper}}{N_{lower}} = exp(\frac{-\Delta E}{kT}) = exp(\frac{-h\nu}{kT}) = \exp(\frac{\gamma h B_0}{2\pi kT})$$

The strength of the signal observed will be

$$S(t) = N_{tot} P sin(\theta) \gamma B cos(\omega t)$$

Where P, the polarization is defined as

$$P = \frac{N_\uparrow - N_\downarrow}{N_\uparrow + N_\downarrow} = \frac{\gamma \hbar B_0}{2kT}$$

At $T = 300K$ and $B_0 = 1T$ for protons we have $P = .0000034$ [**pirl_youtube_mri**]

More generally a sample in thermal equilibrium will have

$$S = \frac{N_{tot}\gamma^3\hbar^2 B_0^2}{4kT}$$

We define the Boltzmann Magnetization M_0 as

$$M_0 = \sum \vec{\mu} \cdot density \cdot P = \frac{N\gamma^2\hbar^2 B_0}{4kT} =_0 B_0$$

1.4 Magnetic resonance

If we apply a B field to a nuclear with magnetic moment that is not already aligned with the field, it will experience Larmor precession. This precession will emit a specific frequency depending on the gyromagnetic ratio and magnitude of the applied B-field, that we can measure. If we apply this perpendicular B-field at the Larmor frequency, we can induce resonance. Thus the spinning nuclei will precess with a frequency proportional to the applied magnetic field, i.e.:

$$\nu_L = \frac{\gamma B_0}{2\pi}$$

1.5 Reference Frames

After the nuclei have been pulsed, their magnetic moments proceed in a corkscrew pattern as they process and reconverge around the baseline magnetic field B_0. This is easier to describe mathematically in a rotating reference frame centered on a nucleus with rotation rate equal to the Larmor frequency. Here we can just look at the behavior of the components of the nucleus magnetic moment in the B_0 and B_1 directions, as one decays and the other approaches μ

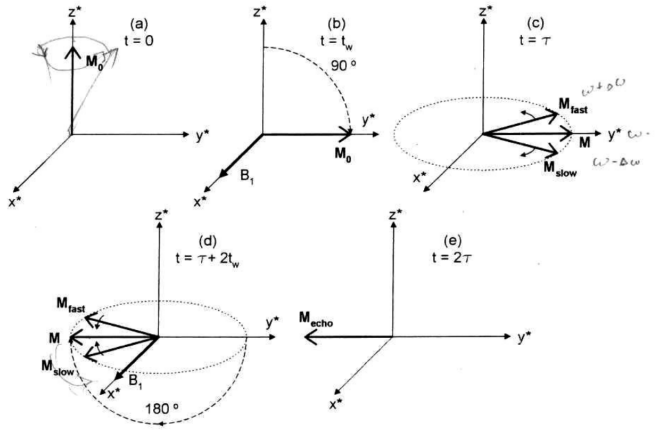

Figure 2: Schematic illustrating each stage of FID [**pulsed_spectrometer_manual**]

1.6 Relaxation times.

Since we need to observe many nuclei in aggregate to have a measurable effect, the nuclei need to all be precessing in phase. They will randomly become out of phase over time after the aligning pulse has been applied due to each other's magnetic fields, and other non-uniform magnetic fields. This leads to the overall signal strength decaying according to the Free Induction Decay (FID).

$$S(t) = Acos(\omega t)e^{-t/T_2}$$

The nuclei will also converge over time back to being in line with the base magnetic field, by the following magnitization

$$M(t) = M_0(1 - e^{-t/T_1})$$

Where T_1 represents the rate at which the nuclei return to allignment with the base magnetid field.

1.7 Bloch equations

The Bloch equations refer to the following electrostatic relations. Definitionally, the torque is the cross product of the magnetic moment with the applied B-field.

$$\vec{T} = \vec{M} \times \vec{B}$$

We also can describe the torque as

$$\vec{T} = \frac{\partial \vec{J}}{\partial \vec{t}}$$

And writing the magnetic moment as the sum of parts, and substituting the gyromagnetic ratio

$$\vec{M} = \sum_i \mu_i = \sum_i \gamma \vec{J}_i$$

$$\frac{\partial \vec{M}}{\partial t} = \gamma \frac{\partial}{\partial t} \vec{J} = \gamma \vec{T} = \gamma (\vec{M} \times \vec{B})$$

When we only have the B_0 field applied along the z-axis, we get the following set of coupled differential equations

$$\frac{\partial}{\partial t} M_x(t) = \gamma M_y B_0 - M_x/T_2$$
$$\frac{\partial}{\partial t} M_y(t) = -\gamma M_x B_0 - M_y/T_2$$
$$\frac{\partial}{\partial t} M_z(t) = -(M_z - M_0)/T_1$$

Which have solutions

$$M_x(t) = [M_x(0)cos(\omega t) - M_y(0)sin(\omega t)]e^{-t/T_2}$$
$$M_y(t) = [M_x(0)sin(\omega t) - M_y(0)cos(\omega t)]e^{-t/T_2}$$
$$M_z(t) = M_{eq} + [M_z(0) - M_{eq}]e^{-t/T_1}$$

1.8 Spin echo

Suppose we give a pulse B_1. Subsequently we apply another pulse with the same magnitude and opposite direction of B_1 at time τ after the first pulse. All the magnetic moments became out of phase due to inhomogeneities in the constant magnetic field. Assuming these inhomogeneities are constant, this second pulse will reverse the trajectory of all these moments, and will reconverge at their initial configuration from the first pulse after another

interval of τ. This reconvergence is known as the **spin echo** and will allow us to measure τ more easily

1.9 T2 and T2* Measurements (spin-spin relaxation)

T2* is the decay rate of the signal when we take into account imperfections in the applied fields. A proton has $\gamma = 42.6MHz/T$, so if we change $B = 1T$ to $B = 1.000001T$ (an error of order 10^{-6}), this can produce a change of

$$\Delta\omega = \gamma\Delta B = 267.5rad/s$$

Assuming our decay is still perfectly exponential with the inhomogeneity, and the effect of the inhomogeneity can be represented as a single exponential term, we have

$$S(t) = S_0 e^{-t/T_2^*} = S_0 e^{-t/T_2} e^{-\gamma\Delta Bt}$$

$$\frac{1}{T_2^*} = \frac{1}{T_2} + \gamma\Delta B$$

(do we need to talk about wy this assumption is valid? The Lorenztian distribution?)

Any magnetic field will have some inhomogeneity, which will put a lower bound on our error no matter how high we raise T_2

1.10 T1 Measurement (spin-lattice relaxation)

Spin lattice relaxation time is our T1 relaxation time, spin-spin is our T2 relaxation time.

The Carr-Purcell method involves applying a 90^o pulse, following by a series of 180^o pulses separated by some time τ, which is short compared to either of the relaxation times. This causes the moments to become coherent again after the diffuse following the first pulse. Repeating this process allows us to see this process multiple times. The Meiboom-Gill enhancement applies a 90^o shift at each successive pulse, which eliminates some of the error accumulation from the Carr-Pucell method

2 Experimental Setup

We will use a light mineral oil and several concentrations of $CuSO_4$ samples and observe it with a TeachSpin PS2-A pulse spectrometer. The sample is positioned in a coil, which is inside the B_0 field. This coil firstly acts as an transmitter, i.e. it supplies a RF wave that changes the net magnetization of the sample. Then, after the signal has been applied, the same coil acts as a "receiver" (pickup coil), and records the precession of the B field in the x-y plane.

The PS2-A Synthesizer module is used to produce the oscillating RF signal that "tips" the spins, altering the net magnetization of the sample. Then the Pulse Programmer module is used to determine the duration and number of the RF pulses. Finally, the Receiver takes care of the amplification of the RF signal going into the coil, and directs the incoming RF resulting from the sample to the oscilloscope.

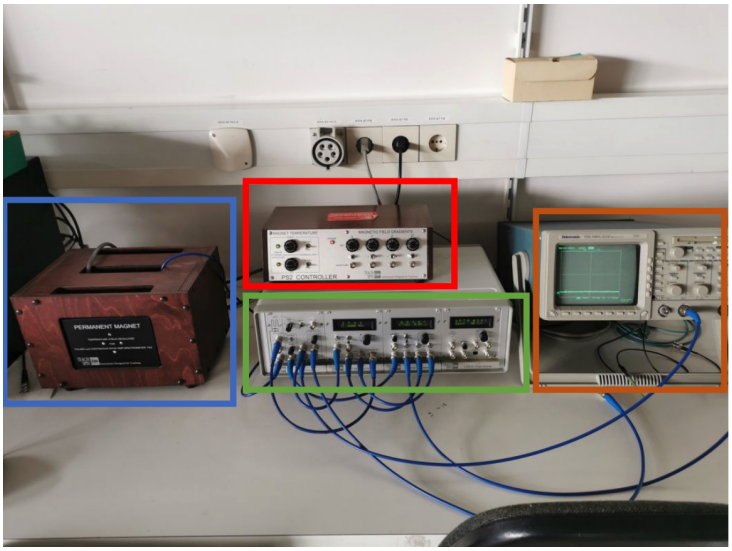

Figure 3: blue box - permanent magnet
red box - magnetic field gradients
green box - spectrometer console including rf synthesizer, pulse programmer and receiver unit
brown box oscilloscope. [**experimental_setup_manual**]

3 Experiment Procedure

We will determine T_1 and T_2 for several concentrations of $CuSO_4$ and a light mineral oil by semi-logarithmic representation of the signal amplitudes over the time.

3.1 Adjusting Parameters

We begin by looking at the FID after applying a 90^o pulse, and do the following

- **Pulse Length Adjustment** We maximize the signal intensity by adjusting the length of the applied pulse
- **Frequency Adjustment** until we've further maximized the intensity, and there are no off-resonance induced oscillations
- Adjust the shimming coils to minimize inhomogeneities
- record T_2 after doing all the above
- Optimize the 180^o pulse by varying tau and other parameters. Here we want to maximize the echo and reduce the second pulse's FID
- Perform Car-Purcell experiment and the Meiboom-Gibson improvement
- Measure T_1 values by building a $180^o - \tau - 90^o$ sequence, varying tau, plotting the FID max, inverting the FID until the zero crossing, and doing an exponential fit.

The resonant frequency for the mineral oil sample was determined to be 21.04581 MHz, and the length of the $\frac{\pi}{2}$ pulse was found to be $\tau_A = 2.8\mu$s and for the π pulse we had $\tau_B = 5\mu$s, which in consistent with the expectation that one should be double the other. However, there was a lot of margin of variation, meaning that the precise value of τ did not have large effects.

4 Determining the Free Induction Decay

In order to determine the Free Induction Decay time T_2^*, we are interested in the signal immediately after the $\frac{\pi}{2}$ pulse, which decays with an envelope of T_2^*. The data for this part was taken from the spin-echo measurements of the following section. Indeed, since multiple spectra for the measurements at different τs were recorded, an average of them was performed, such that it "killed" all the π signals, and only left the average of the $\frac{\pi}{2}$ signal (Figures 4 and 5), with enhanced precision.

This done, we are now interested in the envelope of this resulting decaying signal. It can be described as

$$S(t) = A \cdot e^{-\frac{t}{T_0}}$$

where A is the amplitude, and $T_0 \coloneqq T_2^*$. The fitted parameters were then obtained as ${T_2^*}_{0.1M} = 0.12$ms and ${T_2^*}_{0.2M} = 0.18$ms for the 0.1M and 0.2M concentrations respectively.

So we see a longer decaying time for the higher concentration sample. It was also noticed tat the amplitude of the 0.2M concentration was lower than the 0.1M concontration, which may be counterintuitive because with increasing concentration one would naively expect also an increased signal. More on this will be discussed later.

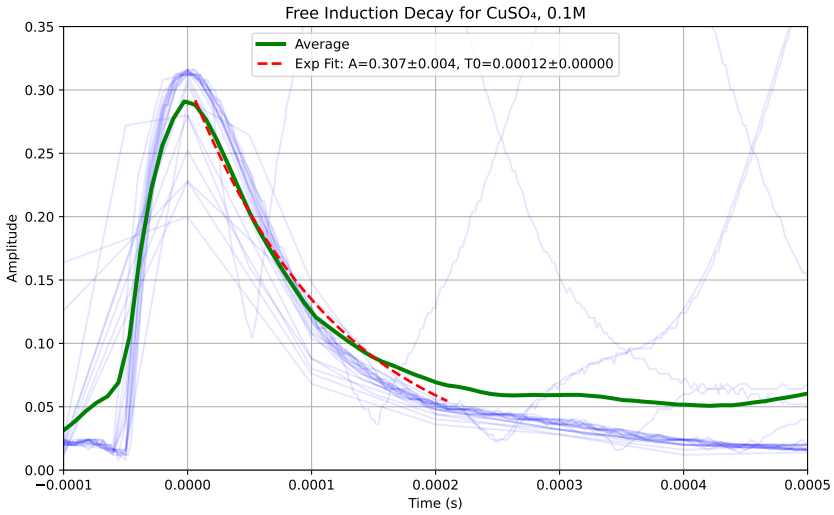

Figure 4: Free Induction Decay measurement for the 0.1M $CuSO_4$ sample. The data was taken from the spin-echo measurements of the following task, and was averaged so as to emphasize the $\frac{\pi}{2}$ pulse. The single measurements are plotted in light blue, and the average in green. A decaying exponential fit was then performed to read off T_2^*.

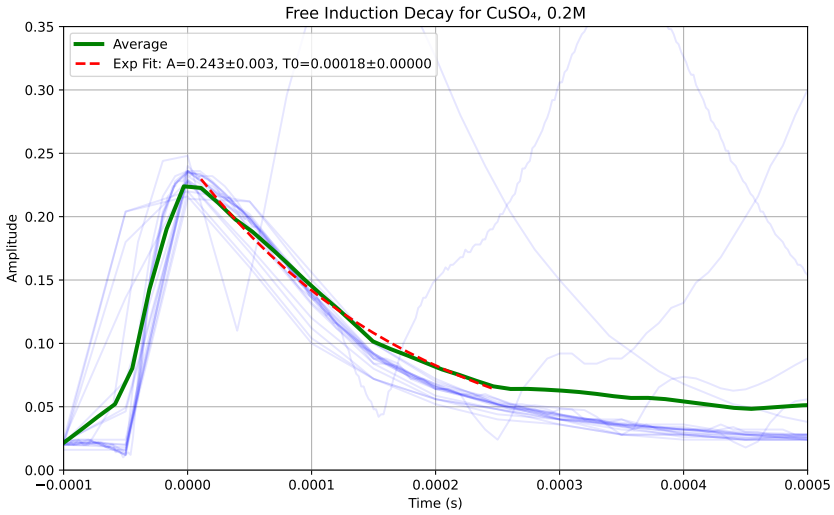

Figure 5: Free Induction Decay measurement for the 0.2M $CuSO_4$ sample. The data was taken from the spin-echo measurements of the following task, and was averaged so as to emphasize the $\frac{\pi}{2}$ pulse. The single measurements are plotted in light blue, and the average in green. A decaying exponential fit was then performed to read off T_2^*.

From the FID, we can then determine the magnetic field inhomegeneity, which, in the approximation $T_2^* \ll T_2$ is given by

$$\Delta B = \frac{\ln 2}{\gamma T_2^*}$$

. Plugging the numbers in (where $\gamma = 42.58 \frac{\text{MHz}}{\text{T}}$, we got for the 0.1M concentration

$$\Delta B \approx 135.6 \mu\text{T}$$

and

$$\Delta B \approx 90.437 \mu\text{T}$$

for the 0.2M concentration.

5 Determining T_2 using three different methods.

5.1 Spin echo method

In order to determine T_2 using the spin-echo method, we are interested in the amplitudes of the echo with respect to time. For this, we first optimized the π pulse by maximizing the echo and minimizing the FID of the second pulse. Then, we varied τ from around 0.0001s to 0.0130s, and plotted the resulting spectra in a single plot, which ensured proper alignment in time. Since different scales of the oscilloscope were used, alignment in time was crucial, and it was performed by manually shifting the $\frac{\pi}{2}$ pulse so that this peaked at time $t = 0$. Then, the peaks of the π pulse were detected for each of the t values (using the `peak_find` function in Python). The height of these peaks decreases exponentially and can then be fit into a decaying exponential function

$$S(t) = A \cdot e^{-\frac{t}{T_2}} + c$$

where A is again, the amplitude, T_2 is the spin-spin relaxation time and c is a shifting factor (irrelevant for our purposes here). The resulting fittings can be seen in Figures 6, 7 and 8, for the 0.05, 0.1 and 0.2M respectively. A trend that is noticeable can be seen by looking at the fitting parameters present in Table **??** - in particular, both T_2 and A decrease for increasing concentrations of the $CuSO_4$ sample.

Parameter	**0.05M**	**0.1M**	**0.2M**
A	0.5973 ± 0.0067	0.4984 ± 0.0034	0.3865 ± 0.0062
T_2 (s)	0.0199 ± 0.0005	0.0101 ± 0.0002	0.0045 ± 0.0002
c	-0.0532 ± 0.0073	0.0056 ± 0.0037	0.0243 ± 0.0068

Table 1: Fit Parameters for Spin-Echo Sequences of $CuSO_4$ at Different Concentrations (Hahn Echo Method)

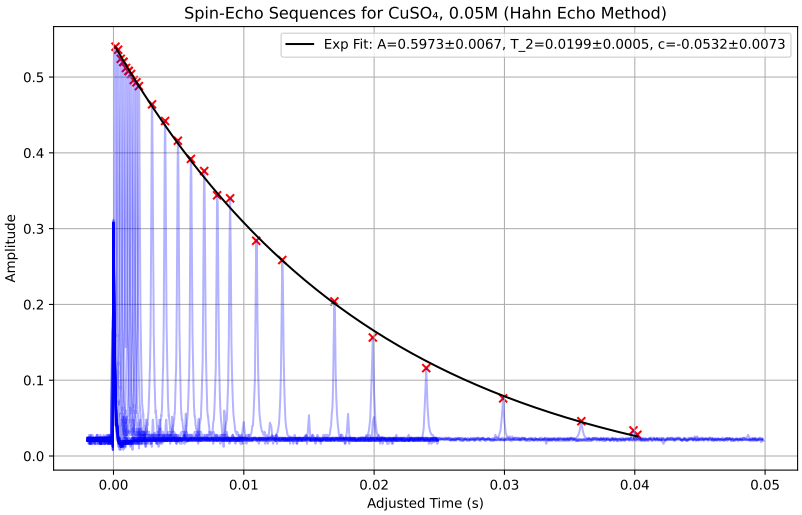

Figure 6: Spin-echo sequences for 0.05M $CuSO_4$ sample. Different values of τ are plotted in light blue, ranging from 0.0001s to around 0.013s.

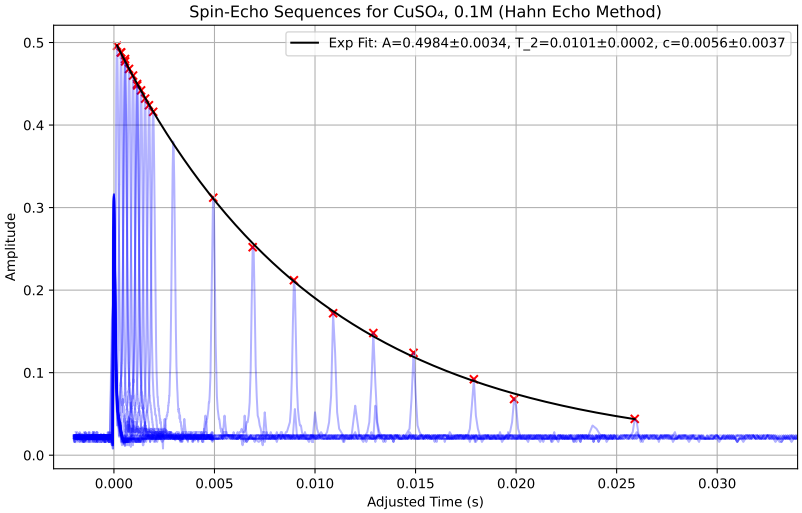

Figure 7: Spin-echo sequences for 0.1M $CuSO_4$ sample. Different values of τ are plotted in light blue, ranging from 0.0001s to around 0.013s.

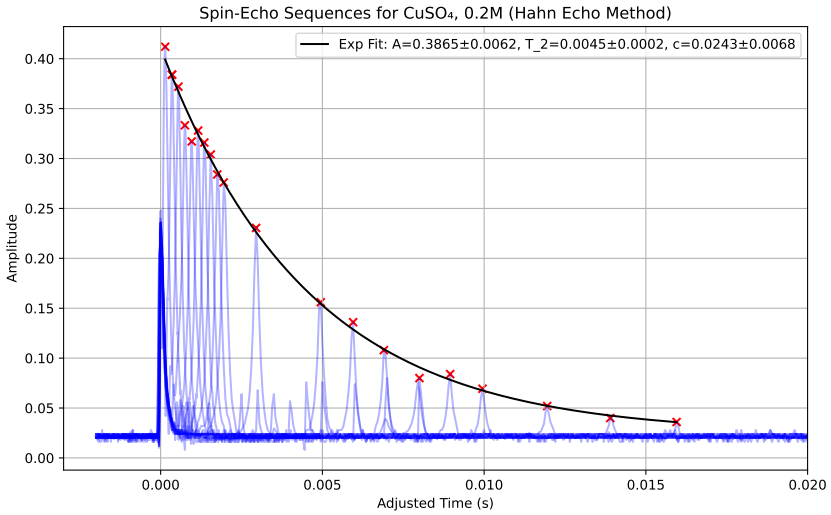

Figure 8: Spin-echo sequences for 0.2M $CuSO_4$ sample. Different values of τ are plotted in light blue, ranging from 0.0001s to around 0.013s.

5.2 Carr-Purcell Method

The principle of this method is the same as the previous one, with the difference that now we are automating the process of shifting τ by initiating a sequence of N spin-echo pulses. In our case, we chose $N = 80$ and $\tau = 0.0001s$.

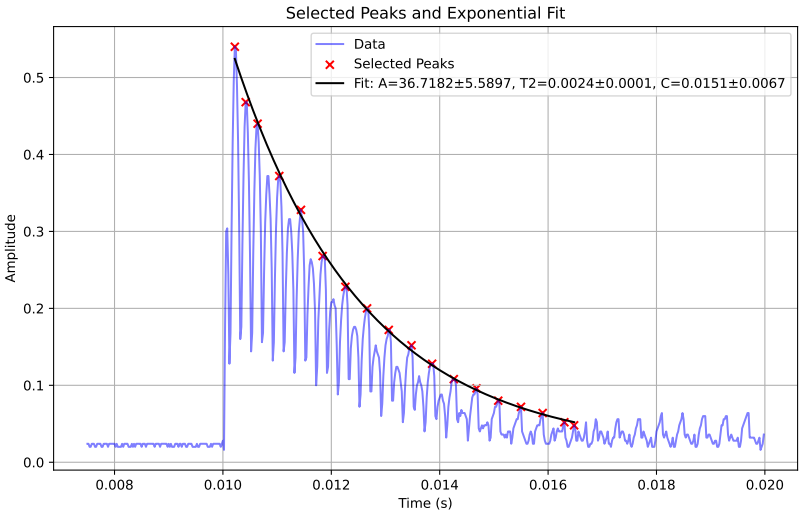

Figure 9: Carr-Purcell method for the 0.05M $CuSO_4$ sample.

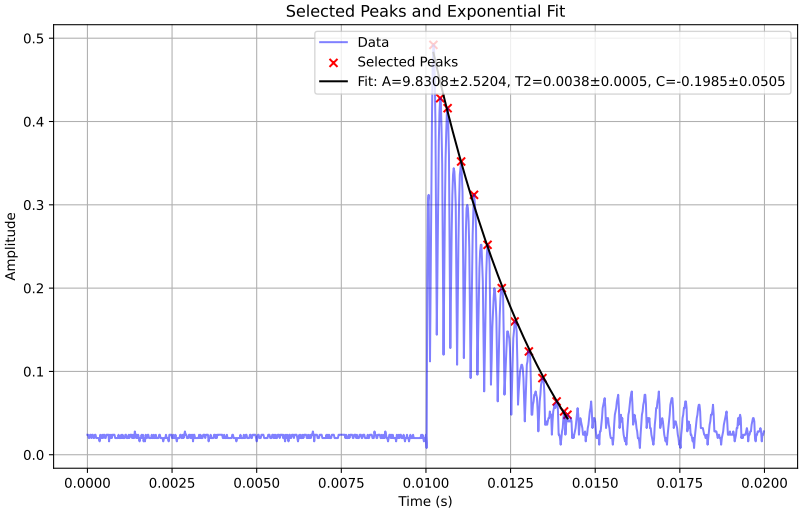

Figure 10: Carr-Purcell method for the 0.1M $CuSO_4$ sample.

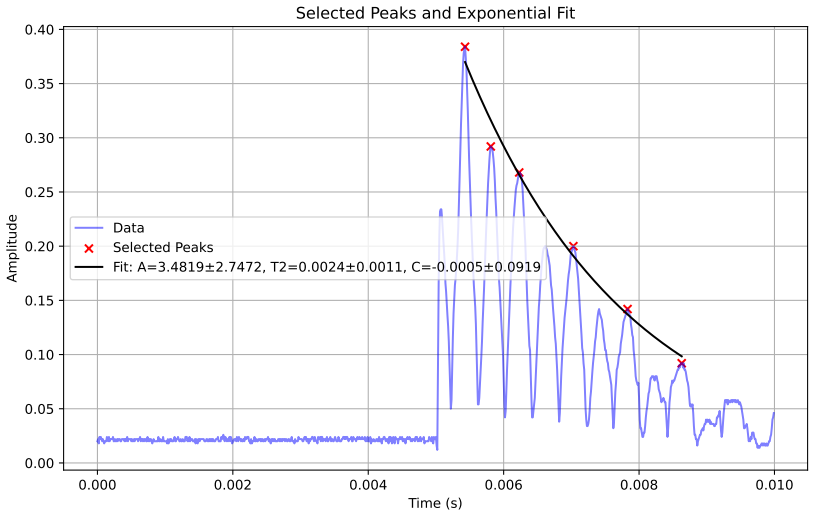

Figure 11: Carr-Purcell method for the 0.2M $CuSO_4$ sample.

5.3 Meiboom Gill Method

To perform the MG measurement, we turned on the MG switch of the setup, which takes care of applying the phase shift between the $\frac{\pi}{2}$ and π pulse, minimizing the flip angle error. Then, we used again N = 80 and $\tau = 0.0001$s to record the spectra for the different concentrations of our sample.

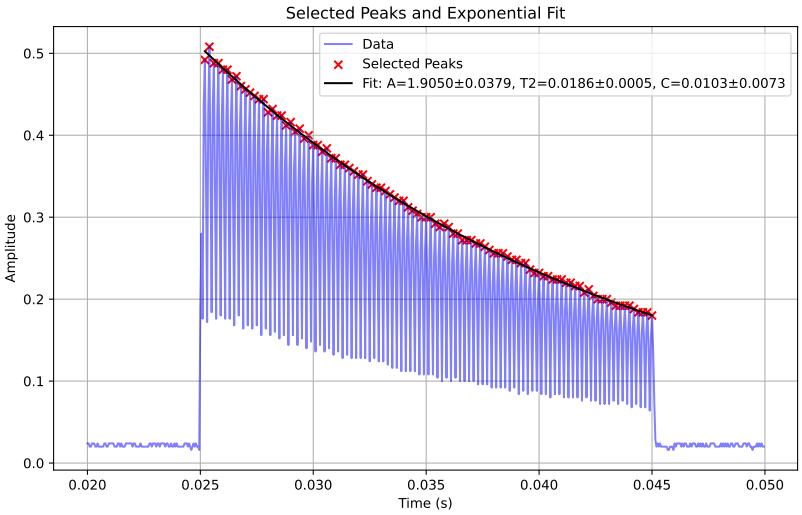

Figure 12: Meiboon-Gill method for the 0.05M $CuSO_4$ sample.

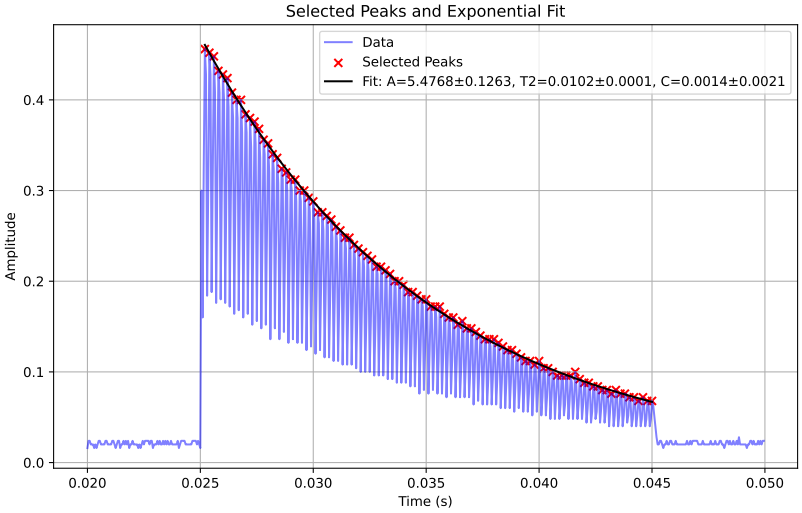

Figure 13: Meiboon-Gill method for the 0.1M $CuSO_4$ sample.

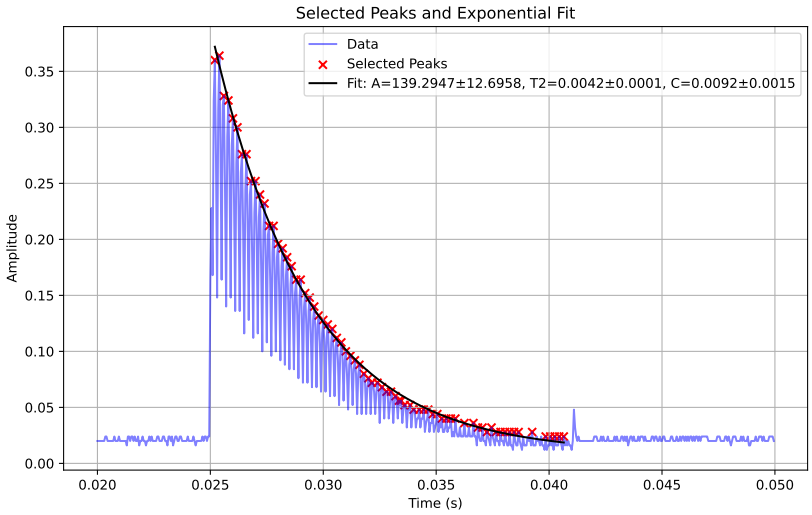

Figure 14: Meiboon-Gill method for the 0.2M $CuSO_4$ sample.

6 Inversion Recovery

Determining T_1 is done via the Inversion Recovery method. This consists in applying a $\pi - \tau - \frac{\pi}{2}$ pulse, at a varying values of τ. We are interested in the amplitude of the signal right after the $\frac{\pi}{2}$ pulse is applied, and how it depends on τ. An effect that needs to be taken into account when performing this task is that the instrument measures the absolute values of the signal, which means that after the inversion pulse, the magnetization is recorded as positive values, even though it's actually decaying toward equilibrium. This leads to an apparent "positive" signal recovery, even though the magnetization itself is recovering in the negative direction initially (after the π pulse). To correct this, we need reverse the sign of the measured signal values after the inversion pulse (i.e., use negative values for the data points), so that the plot correctly represents the recovery of the magnetization toward its equilibrium value. Once the sign is corrected, the exponential recovery can be accurately fit to the function

$$S(t) = A \cdot \left(1 - 2e^{-\frac{t}{T_1}}\right)$$

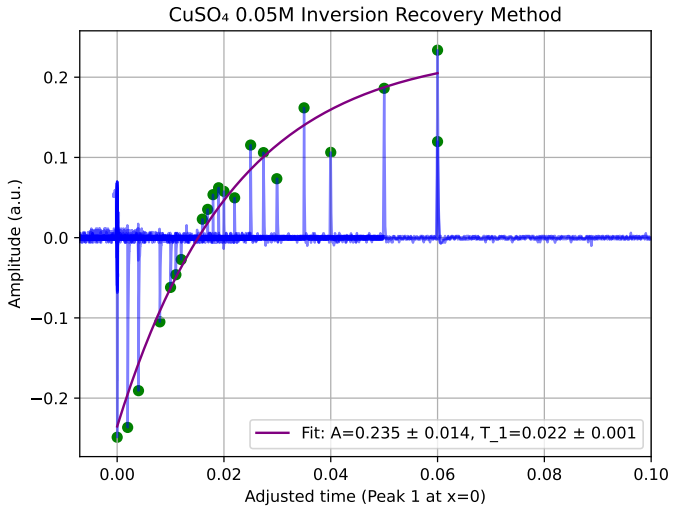

Figure 15: Inversion Recovery method for the 0.05M $CuSO_4$ sample.

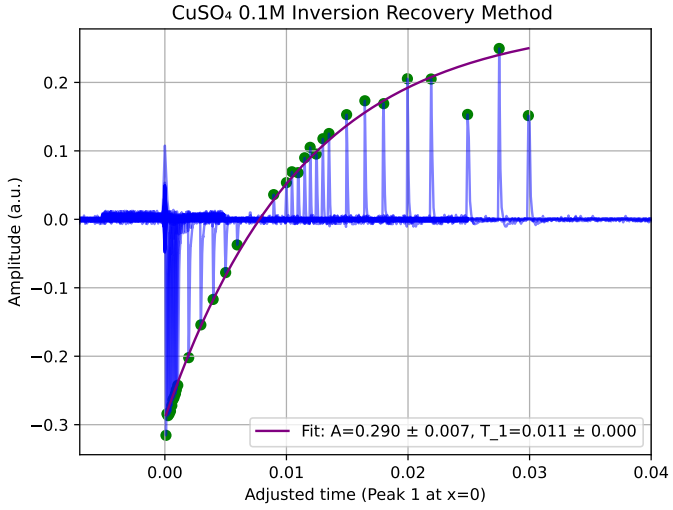

Figure 16: Inversion Recovery method for the 0.1M $CuSO_4$ sample.

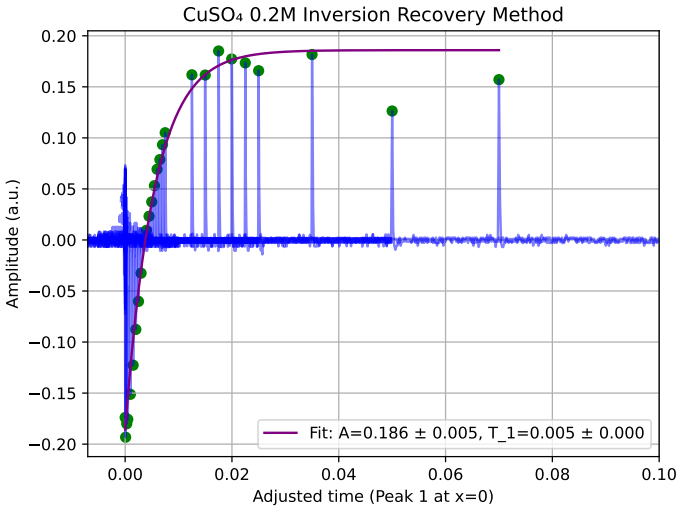

Figure 17: Inversion Recovery method for the 0.2M $CuSO_4$ sample.

6.1 Some Remarks

Table 2 summarizes all the obtained fit parameters for all these methods. From here, we noticed that there was a good consistency between T_2s obtained from the Spin Echo (SE) and Meiboom-Gill (MG) methods, while the Carr-Purcell (CP) method, was less consistent and didn't mostly match. This we believe due to either imperfection on our data, because we used a $N = 80$ which, although we initially believed to be a wise idea, it may have created more noise in the overall data, which made later fitting more difficult. Moreover, the use of $\tau = 0.0001$ was also probably not a happy choice, since this lead to an overlap between the π and $\frac{\pi}{2}$ pulses, which may have somehow biased the data. It is to remark though, that these issues did not occur for the MG method, which suggests that other factors may have caused our issues, but may overall point to the realization that MG method is a big improvement over the CP.

7 Relaxation Times versus Concentrations

The obtained fit parameters for the relaxation times T_1 and T_2 were then plotted against concentration and fitted for each of the employed methods.

Method	Parameter	0.05M	0.1M	0.2M
SE	A (a.u.)	0.5973 ± 0.0067	0.4984 ± 0.0034	0.3865 ± 0.0062
	T_2 (s)	0.0199 ± 0.0005	0.0101 ± 0.0002	0.0045 ± 0.0002
	c	-0.0532 ± 0.0073	0.0056 ± 0.0037	0.0243 ± 0.0068
CP	A (a.u.)	36.7182 ± 5.5897	9.8308 ± 2.5204	3.4819 ± 2.7472
	T_2 (s)	0.0024 ± 0.0001	0.0038 ± 0.0005	0.0024 ± 0.0011
	C	0.0151 ± 0.0067	-0.1985 ± 0.0505	-0.0005 ± 0.0919
MG	A (a.u.)	1.9050 ± 0.0379	5.4768 ± 0.1263	139.2947 ± 12.6958
	T_2 (s)	0.0186 ± 0.0005	0.0102 ± 0.0001	0.0042 ± 0.0001
	C	0.0103 ± 0.0073	0.0014 ± 0.0021	0.0092 ± 0.0015
IR	A (a.u.)	0.235 ± 0.014	0.290 ± 0.007	0.186 ± 0.005
	T_1 (s)	0.022 ± 0.001	0.011 ± 0.000	0.005 ± 0.000

Table 2: Summary of Fit Parameters for Inversion Recovery (IR), Meiboom-Gill (MG), Carr-Purcell (CP), and Spin-Echo (SE) Methods for $CuSO_4$ at Different Concentrations. The C parameters are also shown for completeness, but are not of interest.

The results can be seen in Figure 18 and Table 3. From this, we noticed that there is good consistency between the Spin-Echo (SE) and Meiboom-Gill (MG) methods, which almost coincide, as before, while the CP method diverges, which we attribute to sub-optimal data. In any case, there main trend is a decrease in relaxation time with the concentration increase. The T_1 dependency on concentration shows a similar trend.

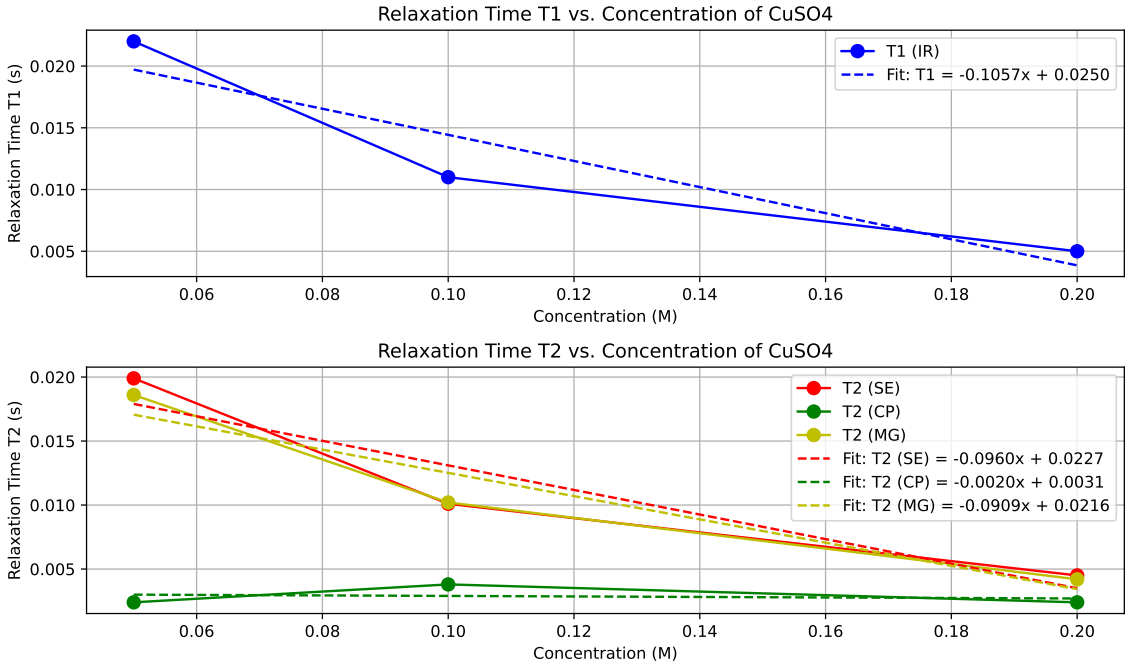

Figure 18: Relaxation times vs. concentrations for all of the methods.

Method	Parameter	Slope (s/M)	Intercept (s)
IR	T1	-0.1057	0.0240
SE	T_2	-0.0960	0.0223
CP	T_2	-0.0020	0.0033
MG	T_2	-0.0909	0.0195

Table 3: Proportionality Factors for Relaxation Times vs. CuSO Concentration

7.1 Proposed Explanation

In NMR, the longitudinal relaxation time T_1 generally decreases with increasing concentration due to enhanced spin-spin interactions. As the concentration increases, the number of nearby spins increases, leading to more

efficient energy transfer between spins, which accelerates the relaxation process. Additionally, higher concentrations can increase local magnetic field inhomogeneities and alter solvent-solute interactions, further facilitating faster relaxation and thus shorter T_1 values.

8 Conclusions

In this report, various techniques were employed to determine the relaxation times T_1 and T_2 for different concentrations of $CuSO_4$ using NMR. The Free Induction Decay (FID) measurements were used to extract T_2^*, with a noticeable trend where the higher concentration sample exhibited a longer decay time, despite a lower signal amplitude. The calculated magnetic field inhomogeneities, derived from T_2^*, were consistent with the expected values for each concentration.

Three methods were used to measure T_2: the Spin Echo (SE), Carr-Purcell (CP), and Meiboom-Gill (MG) methods. While there was good consistency between the SE and MG methods, the CP method showed less consistent results, likely due to experimental issues such as the choice of $N = 80$ and a small τ value. Despite these difficulties, the MG method proved to be the most reliable for measuring T_2 in our experiment.

The Inversion Recovery method was employed to determine T_1, and the resulting data showed a clear trend of decreasing T_1 values with increasing concentration. This is consistent with the expected behavior, as higher concentrations lead to more efficient spin-spin interactions and faster relaxation.

Overall, the obtained relaxation times displayed a clear dependence on concentration, with both T_1 and T_2 decreasing as concentration increased. This suggests enhanced spin interactions at higher concentrations, which was particularly evident in the measured relaxation times for the different methods used.